Materials Transactions, Vol. 47, No. 12 (2006) pp. 2942 to 2949

On the Hardening of Friction Stir Processed Mg-AZ31 Based Composites with 5–20% Nano-ZrO_2 and Nano-SiO_2 Particles

C. I. Chang[1], Y. N. Wang[1,2], H. R. Pei[1], C. J. Lee[1] and J. C. Huang[1,*]

[1]*Institute of Materials Science and Engineering; Center for Nanoscience and Nanotechnology, National Sun Yat-Sen University, Kaohsiung, Taiwan 804, R. O. China*
[2]*Institute of Materials Science and Engineering, Dalian University of Technology, Dalian 116024, P. R. China*

Mg-AZ31 based composites with 10–20 vol% nano-sized ZrO_2 and 5–10 vol% nano-sized SiO_2 particles were fabricated by friction stir processing (FSP). The clusters of the nano-ZrO_2 and nano-SiO_2 particles, measuring 180–300 nm in average, were relatively uniformly dispersed. The average grain size of the Mg matrixes of the composites varied within 2–4 μm after four FSP passes. No evident interfacial product between the ZrO_2 particles and Mg matrix was found during the FSP mixing ZrO_2 into Mg-AZ31. However, significant chemical reactions occurred at the Mg/SiO_2 interface to form the Mg_2Si phase. The mechanical responses of the resulting nano-composites in terms of hardness and tensile properties of these Mg/nano-ZrO_2 and Mg/nano-SiO_2 composites were examined and compared. The grain refinements and the corresponding hardening mechanisms are also analyzed and discussed. [doi:10.2320/matertrans.47.2942]

(Received September 1, 2006; Accepted October 4, 2006; Published December 15, 2006)

Keywords: *friction stir processing; magnesium alloy; nano-sized particles; composite*

1. Introduction

Metal matrix composites (MMCs) have attracted attention due to the increasing need for structural materials with high specific strength and stiffness. In comparison with the aluminum (Al) alloys, magnesium (Mg) alloys have a lower density by 35%, and have exhibited the promise as structural materials in engineering applications which require higher specific mechanical properties. Especially, the aerospace and automobile industries are actively seeking high performance magnesium based alloys. One of the major limitations for Mg and its alloys is their relatively low elastic modulus. However, this limitation can be circumvented by the use of harder and stiffer ceramic particles reinforcements. Improvements in tribological characteristics, dimensional stability, damping capacity, and elevate temperature creep properties can be realized by the proper selection in type, size elastic modulus and volume fraction of the reinforcements. Several methods have been developed to fabricate the particle reinforcement Mg-based composites, including molten metal infiltration,[1)] powder metallurgy,[2)] squeeze casting,[3)] stir casting[4)] and spraying forming.[5)]

Friction-stir welding (FSW) is a solid-state joining process initially developed by The Welding Institute (TWI) in United Kingdom.[6)] This process is characterized by frictional heating and intense material flow originated from the rotation of the welding tool, generally creating an elliptical nugget-shaped stir zone with a fine recrystallized grain structure. Recently, its modification into the friction stir processing (FSP) has also been applied to modify the microstructure by grain size refinements and homogenization of precipitate particles in many aluminum and magnesium alloys.[7–11)] In addition, Mishra *et al.* have mixed a second phase into the matrix via FSP to fabricate surface composites.[12)] Lee *et al.* have mixed nano-SiO_2 powders into the AZ61 magnesium alloy by FSP to successfully fabricate the bulk nano-SiO_2/AZ61 composite.[13)] It appears evident that FSP can offer another feasible route to incorporate ceramic particles into the matrix to form bulk composites.

It is well known that the widely used AZ-series Mg alloys for the enclosures or cases of electronic appliances are typically soft and are prone to the wear problem. The Vicker's hardness (Hv) of the commercial AZ91, AZ61 and AZ31 alloys is usually around 50–65. Our previous efforts by adding 10 vol% (volume fraction) nano-SiO_2 into AZ61 ($Hv \sim 60$) have resulted in the improvement of hardness to a level over 90.[13)] However, the extensive reaction between SiO_2 and Mg makes the hardening unpredictable. In this study, the extension work is presented using the softest AZ31 matrix ($Hv \sim 50$) added with the more stable ZrO_2 nano-particles to 20 vol%. Parallel FSP runs using the SiO_2 nano-particles are also applied for comparison.

2. Experimental Method

The AZ31 billets possessed nearly equiaxed grains around 70 μm was used in this study. The chemical composition (in mass percent) is Mg-3.02%Al-1.01%Zn-0.30%Mn. The samples for FSP were cut from billet as rectangular blocks, measuring 60 mm in width, 130 mm in length and 10 mm in thickness. The crystalline ZrO_2 powders with a monoclinic structure (Fig. 1(a)) and the amorphous SiO_2 powders (Fig. 1(b)) used in this study are nearly equiaxed in shape, with an average diameter $d \sim 20$ nm. The purity levels of these two kinds of powders are both ~99.9% and the densities are 5.89 and 2.65 Mg/m^3, respectively.

The simplified FSP machine is a modified form of a horizontal-type miller, with a 5 HP spindle. The fixed pin tool with 6 mm in diameter and 6 mm in length was used. The shoulder diameter was 18 mm, and the applied tilt angle of the fixed pin tool was 2°. The FSP parameters of advancing speed of 800 rpm and pin rotation of 45 min/min were applied in the present experiment. To insert the nano-particles, one or two grooves (denoted as 1G or 2G) each ~6 mm in depth and 1.25 mm in width were cut, in which the nano-particles were filled to the desired amount before FSP, as shown in Fig. 2. In order to prevent the nano-particles from being displaced out of the groove(s), surface

*Corresponding author, E-mai: jacobc@mail.nsysu.edu.tw

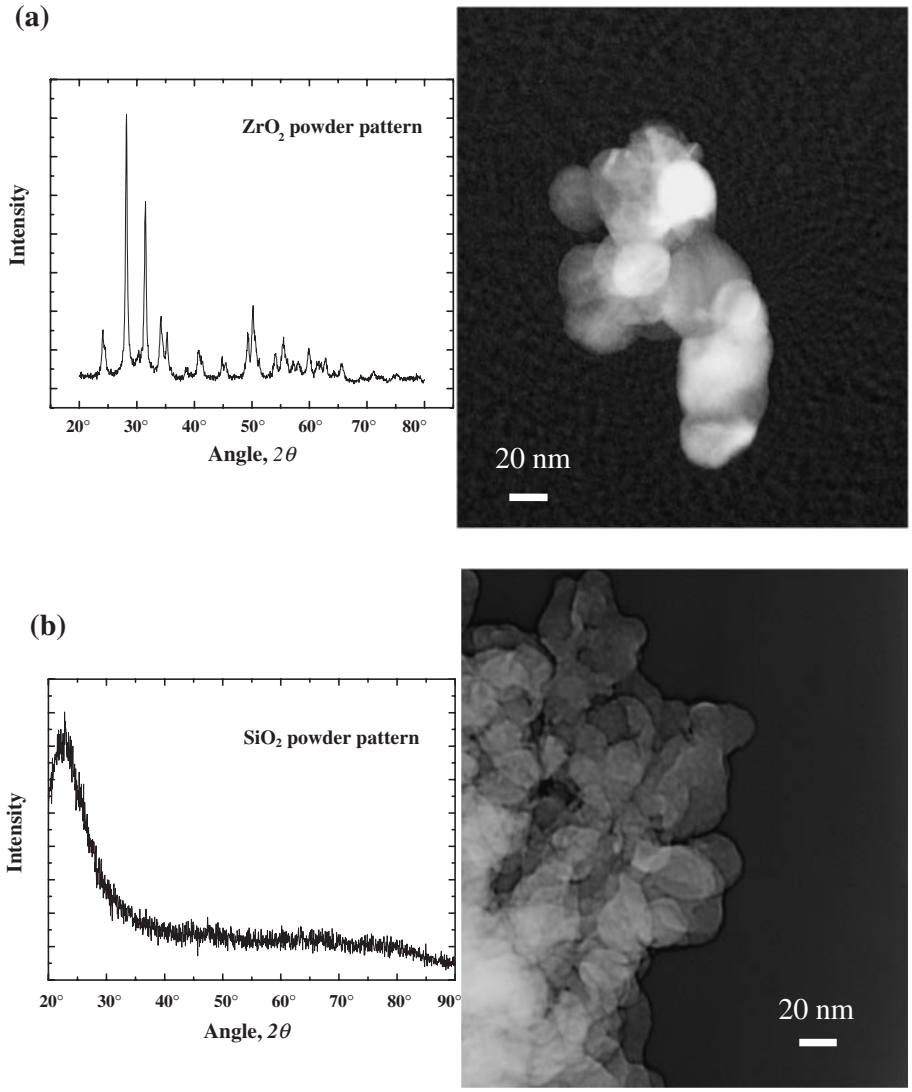

Fig. 1 The XRD patterns and TEM micrographs of (a) the monoclinic ZrO_2 particles and (b) the amorphous SiO_2 particles, both with an average diameter ~20 nm.

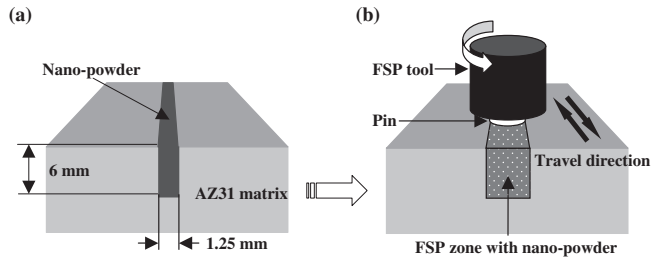

Fig. 2 Schematic drawings of the friction stir process in fabricating the Mg-AZ31/nano-particles composites: (a) cutting groove(s) and inserting nano particles and (b) conducting multiple FSP to fabricate composites.

"repair" was accomplished with a modified FSP tool that only has a shoulder without pin. The details of the FSP procedures are referred in our previous paper.[13] The volume fractions of the ZrO_2 particles in the 1G and 2G composites were calculated and also measured to be ~10 and 20 vol%, respectively; and those of the SiO_2 inserted 1G and 2G composites are ~5 and 10 vol%, respectively. More ZrO_2 nano powders can be inserted into the grooves due to the heavier weight, resulting in about doubling of the particle volume fraction in the ZrO_2 containing composites, as compared with the SiO_2 counterparts. The FSP was conducted for one to four passes (denoted as 1P to 4P), the advancing direction for the subsequent pass was in opposite direction to the previous pass (*i.e.* proceeding in a forward and then backward way).

The Vicker's hardness tests were conducted using a 200 gf load for 10 s. The grain structure and the particle distribution of the etched and unetched samples were examined by optical microscopy (OM), scanning electron microscopy (SEM) and transmission electron microscopy (TEM) with an energy dispersive spectrometer (EDS). The size of clustered nano-particles was analyzed by the Optimas® image analysis software on SEM photographs taken at different magnifications.

3. Results

3.1 Microstructures

Microstructure characterization in this study was mainly focused on the distribution and local clustering of the nano-

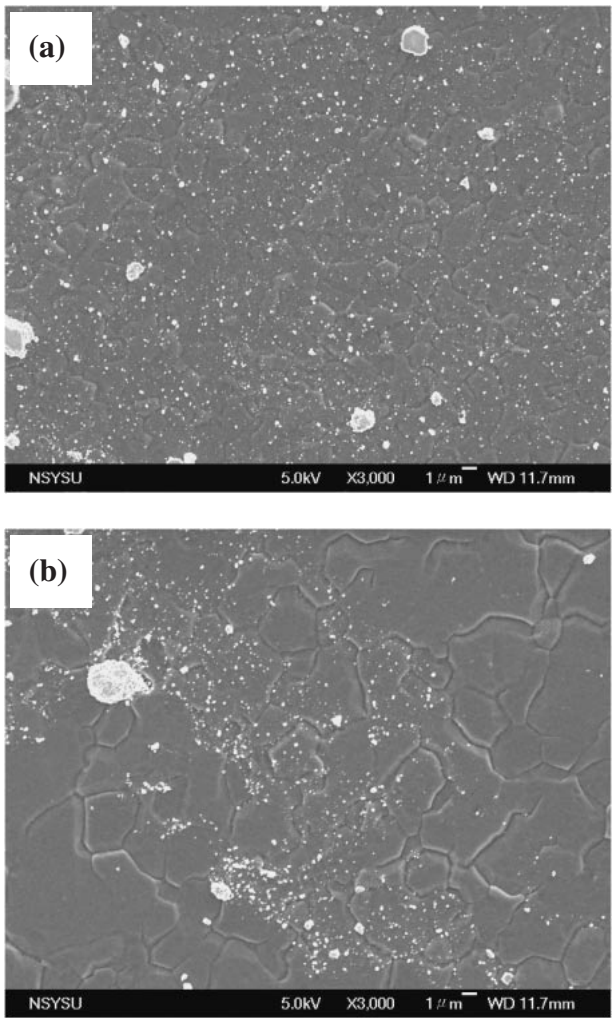

Fig. 3 SEM/SEI images of the AZ31/10 vol%ZrO_2 FSP composite showing (a) relatively homogeneous dispersion, and (b) local inhomogenization of the nano-particle clusters within the stirred zone after one-pass FSP.

ZrO_2 particles, as well as the matrix grain structures in the stirred zone that have undergone dynamic recrystallization. The frictional heating and severe plastic deformation are simultaneously introduced into the stirred material during FSP by the rotating tool. Therefore, it is expected that both the frictional heating and plastic strain would lead to the formation of dynamically recrystallized grains. These two effects would also help in dispersing the inserted nano-ZrO_2 and nano-SiO_2 particles in the stirred zones.

After one-pass (1P) FSP, the dispersion of the nano-particles within the central cross-sectional area of the friction stir zone (FSZ) is basically uniform, as shown in Fig. 3(a). The observed clustered particle size is frequently 0.1–2 μm, much larger than the individual nano-particle size (~20 nm). In addition, some local inhomogeneous areas of the particles can be found in the 1P FSP sample, as shown in Fig. 3(b). The clustered size of the particles after two to four passes (2P to 4P) appears to have further reduced, as shown in Fig. 4. Meanwhile, with increasing FSP passes, the average grain size, d_g, of the AZ31 alloy matrix is also significantly reduced from around 70 μm in the initial billet to 2–4 μm in the 4P FSP samples. At higher magnifications, these clustered particles are generally located on the grain boundaries or triple junctions, and some are embedded inside the grains. The summary of the clustered size of the particles and the average grain size of the AZ31 alloy matrix in the 4P FSP samples are listed in Table 1.

Provided that all of the nano-particles are individually and uniformly dispersed in the alloy, the theoretically estimated particle interspacing $L_s(=(d/2)(2\pi/3f)^{1/2}$, where f is the particle volume fraction),[14] and thus the approximate grain size d_g, should be less than 0.1 μm. It follows that a certain level of local clustering is inevitable, and not all nano-particles can restrict grain boundary migration. Note that the typical grain size of AZ31 alloy (without nano-particles) after the same 4P FSP was measured to be around ~6 μm in our separate studies. The grain size in the FSP composite samples with nano-particles can be refined to $2 \sim 4$ μm, indicating that the nano-particles or clusters in the matrix did play an effective rule in restricting grain boundary migration.

3.2 XRD results

The XRD patterns for the transverses cross-sectional plane of the ZrO_2 and SiO_2 FSP composites are presented in Fig. 5. It can be seen from Fig. 5(a) that in the Mg-AZ31/ZrO_2 composite there is no new phase except for a small amount of the ZrO_2 reinforcement phase (weak peaks) and the Mg matrix. This indicates that the crystalline ZrO_2 phase is very stable, no reaction between the ZrO_2 phase and Mg-AZ31 matrix occurred during FSP. However, some additional weak peaks, identified as Mg_2Si and MgO, can be found in the FSP Mg-AZ31/SiO_2 composite, as shown in Fig. 5(b). It is evident that the chemical reaction between the SiO_2 phase and Mg matrix has occurred during the FSP mixing. The reaction in the Mg-SiO_2 system can be described by the following reaction of $4Mg + SiO_2 \rightarrow 2MgO + Mg_2Si$. Our previous study also confirmed the presence of the Mg_2Si and MgO phases in the Mg-AZ61/nano-SiO_2 composite fabricated by the FSP route.[13]

3.3 Hardness measurements

The typical Vickers hardness readings, Hv, measured along the central cross-sectional zones of the FSP samples are depicted in Fig. 6. Compared with the AZ31 alloy without the ZrO_2 powders reinforcements, almost a double increment of the hardness was achieved for the present composites, especially for the 2G4P sample with ~20 vol% ZrO_2 particles, as seen in Table 2. After FSP, the scattering of Hv within the FSP nugget zone is considered to be relatively minor, implying that the pin stirring has efficiently dispersed the nano-ZrO_2 particles in a reasonably uniform manner, especially after more than one pass. In comparison, the SiO_2 containing composites show lower Hv, mainly a result of the lower particle volume fraction. For the AZ31 alloy without any ZrO_2 reinforcement, after four passes FSP, the Hv could also increase from ~50 for the AZ31 billet up to ~70, due to the grain refinement from ~70 μm down to ~6 μm via dynamic recrystallization.

3.4 Mechanical properties

All tensile samples were machined perpendicular to the processing direction from the central region of the FSP

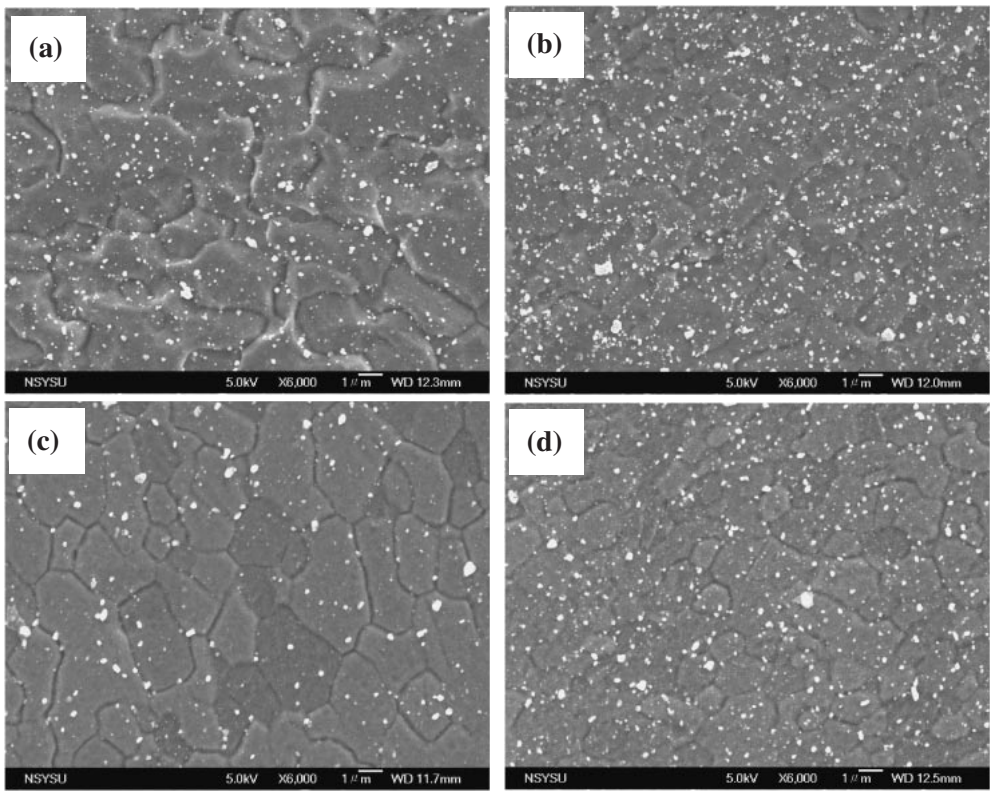

Fig. 4 SEM/SEI micrographs showing the ZrO_2 particle dispersion with (a) ~10 vol%, and (b) ~20 vol% particles, and the SiO_2 particle dispersion with (c) ~5 vol%, and (d) ~10 vol% particles after 4-pass FSP.

Table 1 Summary of the average cluster size of nano-particles and the average grain size of AZ31 matrix in the 4 passes FSP composites.

Materials	AZ31 after 4P	AZ31/ZrO_2 (~10%)	AZ31/ZrO_2 (~20%)	AZ31/SiO_2 (~5%)	AZ31/SiO_2 (~10%)
Average grain size (μm)	~ 6	~ 3	~ 2	~ 4	~ 3
Particle cluster size (nm)		~ 200	~ 180	~ 300	~ 260

nugget. Table 2 also lists the tensile properties of the AZ31 FSP alloy and composites, taking the average from two or three samples. For the AZ31 billet without FSP, the room-temperature yield strength (*YS*), ultimate tensile strength (*UTS*), and tensile elongation are ~100 MPa, 160 MPa, and 9%, respectively. After 4P FSP for the AZ31 billet, they are improved to ~120 MPa, 204 MPa, and 18%. The increase of *YS* and *UTS* as well as elongation for the FSP AZ31 sample was mainly contributed by the grain refinement.

For the FSP composites, the *YS* and *UTS* were improved also by the nano-particle reinforcements, in addition to the apparent grain refinement. For example, the yield stress of the Mg-AZ31/ZrO_2 FSP composites was improved to 143 MPa in the 1G4P (~10% ZrO_2) and to 167 MPa in the 2G4P (~20% ZrO_2) samples. The ultimate tensile strength is also appreciably improved in parallel. The increment of *YS* and *UTS* for the SiO_2 containing composites was slightly lower, due to the lower particle volume fraction. Note that the *YS* and *UTS* values of the FSP AZ31 alloy and composites specimens are all lower than those observed in the extruded or rolled AZ31 materials possessing similar fine grain sizes of 2–6 μm.[15,16] This is mainly a result of the special texture effect addressed elsewhere.[17]

The differences in the fracture behavior between the FSP Mg-AZ31 alloy and the particle reinforced composites can be seen from the SEM fractographs in Fig. 7. The fracture surface of the FSP AZ31 alloy exhibits elongated uniform dimples, as shown in Fig. 7(a), which indicate the overall ductile fracture mode with a tensile elongation of 18%. In contrast, the fracture behavior of the present composite, for example, Mg-AZ31/10%ZrO_2, is very different, as shown in Fig. 7(b). Some dimples with the clusters of ZrO_2 particles, and some round and shallow small dimples in the matrix area can be seen on the fracture surface of the composite. The more shallow dimples indicate a relatively more brittle fracture mode with a tensile elongation of 6%.

4. Discussion

Predicting the overall mechanical properties of the composite is very important for material designs and applications. There have been many attempts to correlate

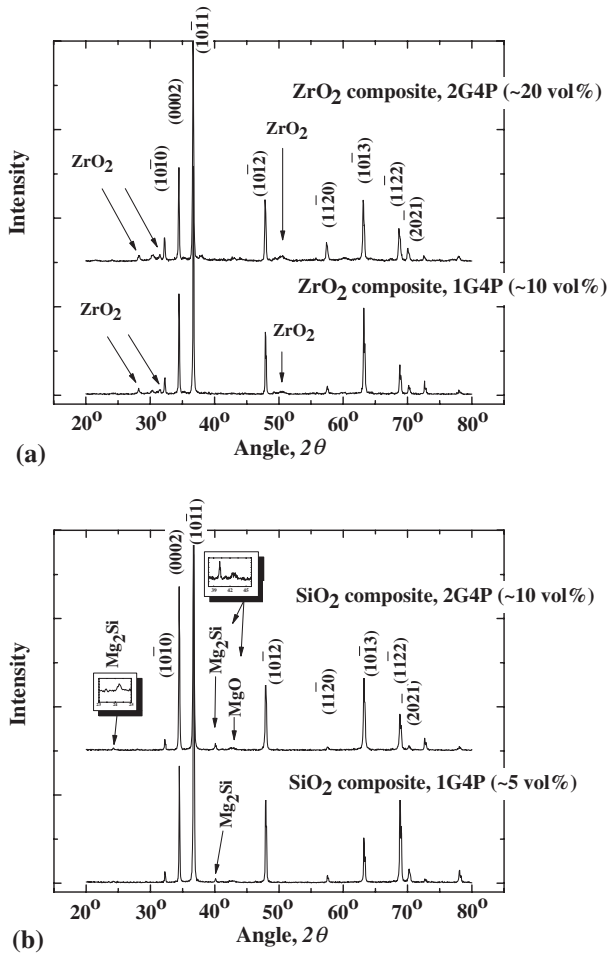

Fig. 5 XRD patterns for (a) the Mg-AZ31/ZrO_2 and (b) the AZ31/SiO_2 composites.

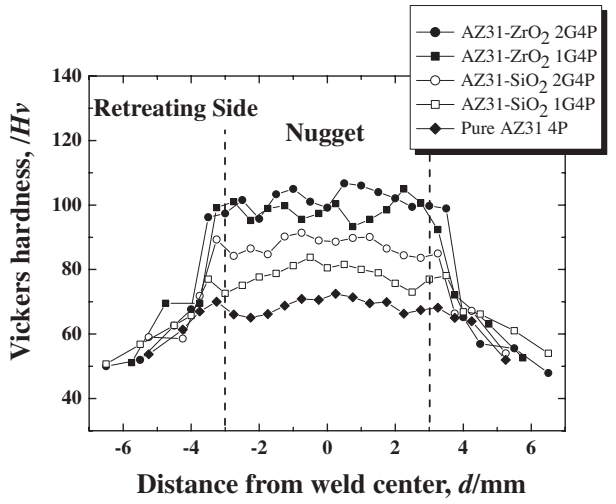

Fig. 6 Typical variations of the microhardness (*Hv*) distribution in various FSP AZ31 composites and the FSP AZ31 alloy (no particles).

the overall composite mechanical properties with the properties of the composite constitutes, for example, the self-consistent variation methods,[18] mean-field theories,[19] shear-lag theory,[20] finite element method (FEM)[21] and the rule of mixtures (ROM).[22] Among them, the simplest and intuitive

Table 2 Comparison of the mechanical properties of AZ31 alloy and AZ31-based composites.

Materials	*Hardness*/*Hv*	*YS*/MPa	*UTS*/MPa	*El* (%)
AZ31 billet	50	100	160	~ 9
AZ31 after 4P FSP	69	120	204	~ 18
~10 vol% ZrO_2 (1G4P)	98	143	232	~ 6
~20 vol% ZrO_2 (2G4P)	105	167	255	~ 6
~5 vol% SiO_2 (1G4P)	78	—	—	—
~10 vol% SiO_2 (2G4P)	87	128	258	~ 6

YS: yield strength; *UTS*: ultimate tensile strength; *El*: elongation.

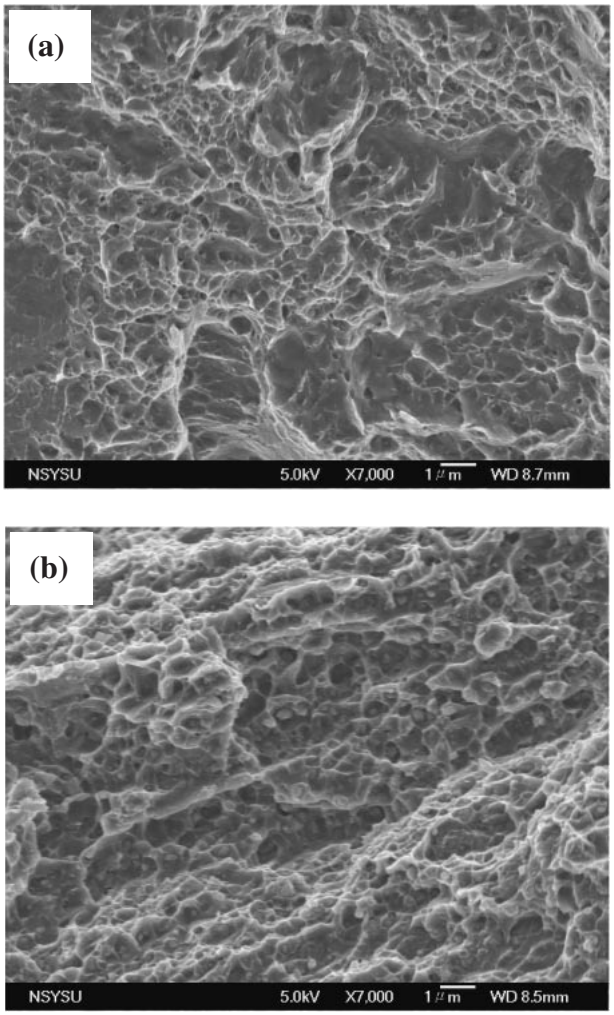

Fig. 7 SEM/SEI fractographs of tensile samples: (a) the FSP AZ31 alloy, and (b) the FSP AZ31/10%ZrO_2 composite.

method for estimating the effective mechanical properties in terms of constitutes is the ROM. Although the FEM gives satisfactory results for problems with the complex geometry and the nonlinearity of the materials properties, the ROM as a simple and fast solution for the simplified model is also useful, in which, the Voigt model based on the equal stain assumption and the Reuss model based on the equal stress assumption have been widely used.

However, most of the models are derived for elastic properties. In addition, the correlation between the effective hardness of the composite, which is the easiest mechanical

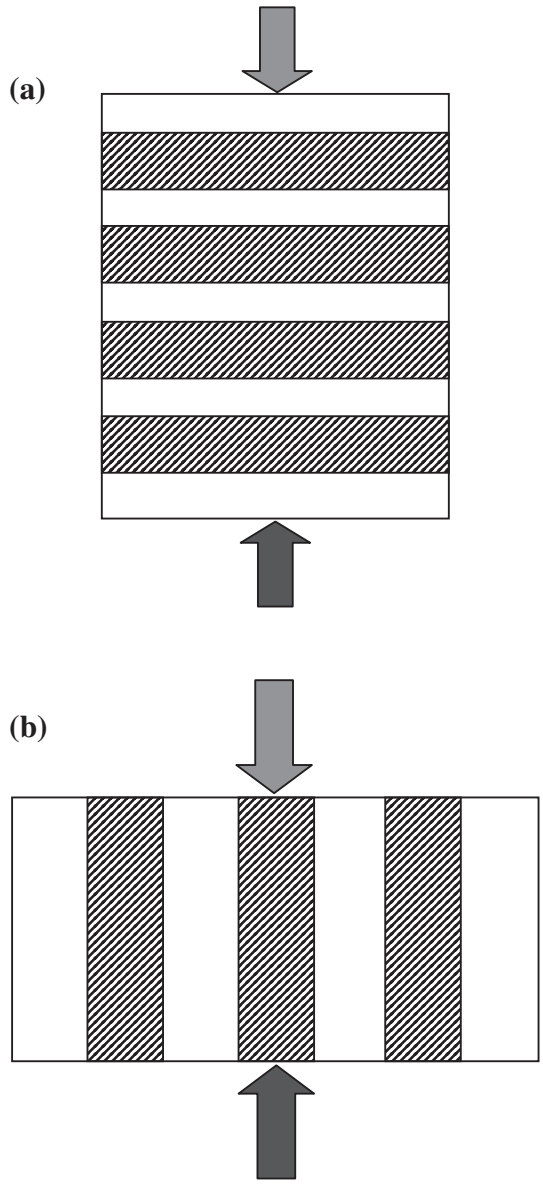

Fig. 8 Schematic diagrams showing (a) the iso-stress and (b) the iso-strain models.

property obtained by simple testing, and the hardness values of its constituent phases are not well established. Therefore, there is still argument about the validity of the ROM for composites with hard particles, especially for plastic properties.

Figure 8 shows a schematic diagram showing (a) the iso-stress (Reuss) model and (b) the iso-strain (Voigt) model. The ROMs, such as the equal strain treatment which is an upper bound, eq. (1) below, and the equal stress treatment which is a lower bound, eq. (2) below, can be used for estimating the effective hardness $\bar{H}$ of the composite:

$$\bar{H}_{up} = f_h H_h + f_s H_s, \tag{1}$$

$$\bar{H}_{low} = (f_h/H_h + f_s/H_s)^{-1}, \tag{2}$$

where, H_h and H_s are the hardness values of the hard and soft phases, and f_h and f_s are the volume fractions of the hard and soft phases, respectively. The subscripts up and low in $\bar{H}$ represent the upper and the lower bounds of hardness, respectively.

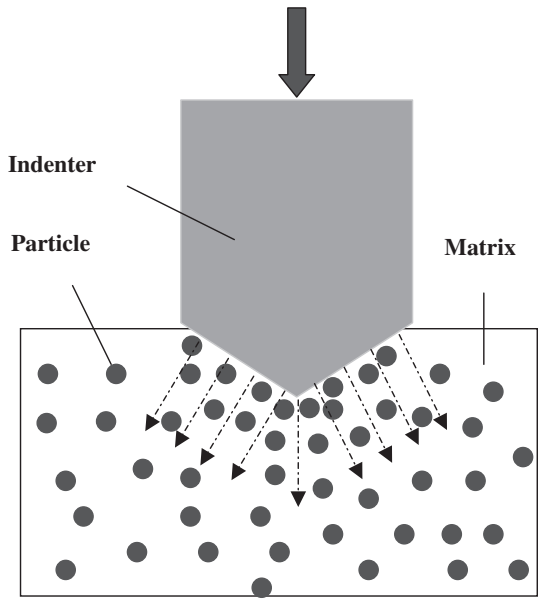

Fig. 9 Schematic drawing of the load transfer direction under the indentation test.

More recently, the elastio-plastic finite element analysis (FEA) for the conventional unit cell model of the uniaxial compression of the composites with homogeneously distributed second particles has been carried out by Kim.[23] Combined with experimental results, the validity of the ROM in composites with hard particles had been confirmed. The FEA results fit better with the iso-strain model except for low volume fractions (<30%) of hard particles where the FEA results fit closely the iso-stress curve. This can be explained by the fact that the deformation of the soft matrix is larger than that of the hard particle. That is, as the compression proceeds on a composite with a high volume fraction of the hard particles, the distance between the particles is getting closer, the load is transferred to the adjacent particles along the loading direction and the hard particles can be deformed. On the other hand, for a low volume fraction of the hard particles, the deformation occurred mainly in the soft matrix with little deformation of the hard particles. Such inhomogeneous deformation with the main deformation occurring in the soft matrix is much more apparent under the indentation of the composite than under the uniaxial compression. Figure 9 shows a schematic drawing of the load transfer direction in the indentation test. Because the loading direction is mainly normal to the indenter surface, the stress state might be similar to the 'iso-stress' condition rather than the 'iso-strain' condition.

The extreme case of this inhomogeneous deformation is the 'wet sand effect',[24] which means that only the soft matrix surrounding the hard particles deforms. In this case, it might be considered that the effective hardness of the particle reinforced composite is mainly related to the hardness of the soft matrix. This situation can be analyzed by using the following approximation of the 'iso-stress' case,

$$\bar{H}_{low} = H_h H_s/(f_h H_s + f_s H_h) \approx H_s/f_s, \tag{3}$$

when $H_h \gg H_s$ and $f_h \ll f_s$.

Equation (3) indicates that the effective hardness of the

Table 3 The experimental hardness and predicted hardness used by the iso-stress model in the present composites. The initial hardness for the AZ31 billet is ~50.

Particle and its volume fraction in composite	Measured hardness of composite, Hv	Hardness of matrix*, Hv	Predicted hardness of composite, Hv
~10 vol% ZrO_2	98	82 ($d_g \sim 3\,\mu m$)	96
~20 vol% ZrO_2	105	90 ($d_g \sim 2\,\mu m$)	112
~5 vol% SiO_2	78	76 ($d_g \sim 4\,\mu m$)	80
~10 vol% SiO_2	87	82 ($d_g \sim 3\,\mu m$)	96

*The matrix hardness is calculated by the equation $H_v = 40 + 72d_g^{-1/2}$.[11]

particle reinforced composite can be approximated to that of the soft matrix only when the hardness of the hard particle is much higher than that of the soft matrix ($H_h \gg H_s$) and the volume fraction of the particles is much lower than that of the matrix ($f_h \ll f_s$). Otherwise, this approximation, eq. (3), is not satisfied and should be modified.

In the present ZrO_2 and SiO_2 particle reinforced Mg-AZ31 composites fabricated by FSP, it is hardly possible to prepare the same state of the matrix in the real samples, regardless of the volume fraction of the same-sized particles. However, the hardness of the matrix without any particle can be roughly deduced from our previous results:[11]

$$H_v = 40 + 72{d_g}^{-1/2}. \quad (4)$$

The comparison of the hardness of the AZ31 matrix deduced from Eq. (3) is given in Table 3. The hardness Hv of the ZrO_2 and SiO_2 particles is ~900 and ~1000, respectively, much higher than that of the AZ31 matrix after FSP ($Hv \sim 76$–90, depending on the refined grain size). The maximal volume fraction of the particles is ~20%. Therefore, it is considered that the approximation of eq. (3) is satisfied for the present case. The prediction results, as shown in Table 3, approximately match the experimental ones, especially in the case of lower volume fractions. Our present results confirm that the effective hardness of the particle reinforced composite can be approximated to that of the soft matrix when the hardness of the hard particle is much higher than that of the soft matrix and the volume fraction of the particles is much lower than that of the matrix.

As can be seen in Table 1, the average grain size of the FSP composites is smaller than that of the un-reinforced FSP Mg-AZ31 alloy. The finer grain structure in the composites could result from the SiO_2 or ZrO_2 particle addition. It is well recognized that the second phase particles will influence the stress and strain distribution during plastic deformation, and thus particles will strongly affect the dynamic recrystallization (DRX) process. Generally, particles could be classified into two size groups according to their effects on RX. Particles larger than 0.1–1 μm will stimulate the RX process, while particles smaller than 0.1 μm will hinder DRX process.[25]

As for the present composites, the behavior of the second phases might be much more complex since their size and distribution will change during FSP. During the first FSP, the particles will be dispersed inhomogeneously, some large size particle clusters will occur unavoidably. However, the particles will be dispersed more and more homogeneously with increasing FSP passes, and the large size particle clusters will change into smaller ones gradually (to an average size of 180–300 nm, as listed in Table 1). Simultaneously, stress concentration around the second phases (particle clusters) will produce a large strain gradient in the adjacent magnesium matrix because of the dislocation pile-up against the second phases during the FSP deformation. Nucleation of dynamic recrystallization is stimulated in these zones. While the nuclei grows, small second phases will hinder grain boundary migration due to the Zener pinning. The second phase pinning on grain boundaries could be observed clearly in Fig. 4. In other words, the second phases play a different role in DRX during FSP according to their changing size. At the beginning of FSP, while the second phase is large, the strain energy in the matrix around it is high. These kinds of places are preferential sites for nucleation of DRX. While the second phase changes into small particles due to the mechanical breaking with increasing FSP passes, the new nuclei has already been produced in the matrix. Then, the small particles act as obstacles for grain growth. Therefore, relatively fine magnesium grains are generated in the present composites during the multiple FSP passes. If the FSP heat input is lowered by lowering the pin rotation and raising the advancing speed, the resulting grain size can be further lowered.

In this study, it is clear that the softest AZ31 Mg alloy can be hardened by the inclusion of nano fillers through FSP, from $Hv \sim 50$ up to $Hv \sim 105$. If the harder AZ91 alloy is in use, Hv is expected to be raised from the original 65 to over 120, based on the prediction of H_s/f_s in eq. (3). The hardened bulk section or surface layer would greatly improve the wear resistance that is vital for practical applications.

5. Conclusions

(1) Friction stir processing successfully fabricated bulk Mg-AZ31 based composites with 10–20 vol% of nano-ZrO_2 particles and 5–10 vol% of nano-SiO_2 particles. The distribution of the 20 nm nano-particles after four FSP passes resulted in satisfactorily uniform distribution.

(2) The average cluster sizes of the nano-ZrO_2 and nano-SiO_2 particles after four FSP passes are around 150–200 and 200–300 nm, respectively. The average grain size of the AZ31 matrix of the 4P FSP composites could be effectively refined to 2–4 μm, as compared with the ~6 μm in the FSP AZ31 alloy (without particles) processed under the same FSP condition. The crystalline ZrO_2 phase is very stable, no reaction between ZrO_2 and Mg phases occurred during the FSP mixing.

(3) The hardness and tensile properties at room temperature

of the AZ31 composites with nano-fillers were improved (up to $Hv \sim 105$), as compared with the AZ31 cast billet ($Hv \sim 50$). The hardened bulk section or surface layer would greatly improve the wear resistance that is vital for practical applications.

(4) The effective hardness of the present particle reinforced composites can be approximately predicted by the iso-stress model when the hardness of the hard particle is much higher than that of the soft matrix and the volume fraction of the particles is much lower than that of the matrix.

Acknowledgements

The authors would like to gratefully acknowledge the sponsorship from National Science Council of ROC under the projects NSC 93-2216-E-110-021 and 94-2216-E-110-010. The author Y. N. Wang is also grateful to the post-doc sponsorship from NSC under the contract NSC 94-2811-E-110-004.

REFERENCES

1) B. Q. Han and D. C. Dunand: Mater. Sci. Eng. A **277** (2000) 297–304.
2) D. M. Lee, S. K. Suh, B. G. Kim and J. S. Lee: Mater. Sci. Tech. **13** (1997) 590–595.
3) L. Hu and E. Wang: Mater. Sci. Eng. A **278** (2000) 267–271.
4) R. A. Saravanan and M. K. Surappa: Mater. Sci. Eng. A **276** (2000) 108–116.
5) C. Y. Chen and Chi Y. A. Tsao: Mater. Sci. Eng. A **383** (2004) 21–29.
6) W. M. Thomas, E. D. Nicholas, J. C. Needham, M. G. Church, P. Templesmith and C. J. Dawes: Intl. Patent No. PCT/GB92/02203.
7) R. S. Mishra, M. W. Mahoney, S. X. McFadden, N. A. Mara and A. K. Mukherjee: Scripta Mater. **42** (2000) 163–168.
8) Z. Y. Ma, R. S. Mishra and M. W. Mahoney: Acta Mater. **50** (2002) 4419–4430.
9) P. B. Berbon, W. H. Bingel, R. S. Mishra, C. C. Bampton and M. W. Mahoney: Scripta Mater. **44** (2001) 61–66.
10) D. T. Zhang, M. Suzuki and K. Maryam: Scripta Mater. **52** (2005) 899–903.
11) C. I. Chang, C. J. Lee and J. C. Huang: Scripta Mater. **51** (2004) 509–514.
12) R. S. Mishra, Z. Y. Ma and I. Charit: Mater. Sci. Eng. A **341** (2003) 307–310.
13) C. J. Lee, J. C. Huang and P. J. Hsieh: Scripta Mater. **54** (2006) 1415–1420.
14) A. J. Ardell: Metall. Trans. **16A** (1985) 2131–2165.
15) H. K. Lin and J. C. Huang: Trans. **43** (2002) 2424–2429.
16) Y. N. Wang, C. J. Lee, H. K. Lin, C. C. Huang and J. C. Huang: Mater. Sci. Forum **426–432** (2003) 2655–2659.
17) Y. N. Wang, C. I. Chang, C. J. Lee, H. K. Lin and J. C. Huang: Scripta Mater. **55** (2006) 637–640.
18) P. Leble, M. Dong, E. Soppa and S. Schmauder: Scripta Mater. **38** (1998) 1327–1332.
19) O. B. Pederson: Acta Metall. **31** (1983) 1795–1808.
20) V. C. Nardone and K. M. Prewo: Scripta Metall. **20** (1986) 43–48.
21) M. Dong and S. Schmauder: Acta Mater. **44** (1996) 2465–2478.
22) R. Hill: Phys. Soc. Lond. A **65** (1952) 349–354.
23) H. S. Kim: Mater. Sci. Eng. A **289** (2000) 30–33.
24) Z. C. Zhong, X. Y. Jiang and A. L. Greer: Philos. Mag. **76** (1997) 505–510.
25) N. Hansen and D. J. Jensen: *Recrystallization'90. Australia*, ed. by T. Chandra, (The Mineral, Metals and Materials Society; 1990) p. 79–88.